

Mechanical properties of medium-temperature thermoelectric materials based on tin and lead tellurides

Mikhail G. Lavrentev¹, Mikhail V. Voronov², Aleksey A. Ivanov², Viktoriya P. Panchenko², Nataliya Yu. Tabachkova³, Maksim K. Tapero^{3,4}, Ivan Yu. Yarkov^{1,4}

¹ RMT Ltd., 46 Warszawskoe Highway, Moscow 115230 Russian Federation

² National Research Centre “Kurchatov Institute”, 1 Kurchatov Sq., Moscow 123182 Russian Federation

³ Prokhorov General Physics Institute of the Russian Academy of Sciences, 38 Vavilov Str., Moscow 119991, Russian Federation

⁴ National University of Science and Technology “MISIS”, 4-1 Leninsky Ave., Moscow 119049, Russian Federation

Corresponding author: Nataliya Yu. Tabachkova (ntabachkova@gmail.com)

Received 3 November 2023 ♦ Accepted 14 November 2023 ♦ Published 12 December 2023

Citation: Lavrentev MG, Voronov MV, Ivanov AA, Panchenko VP, Tabachkova NYu, Tapero MK, Yarkov IYu (2023) Mechanical properties of medium-temperature thermoelectric materials based on tin and lead tellurides. *Modern Electronic Materials* 9(4): 185–192. <https://doi.org/10.3897/j.moem.9.4.116423>

Abstract

The strength and thermoelectric properties of PbTe and Sn_{0.9}Pb_{0.1}Te medium-temperature polycrystalline specimens with *p* and *n* conductivity types, respectively, have been studied. The specimens have been produced using extrusion and spark plasma sintering. The strength parameters of the materials were studied using uniaxial compression at 20 to 500 °C. The structure of the materials was studied using X-ray diffraction and electron microscopy. The electrical conductivity and the Seebeck coefficient were measured simultaneously using the four-probe and differential methods. The temperature conductivity and the specific heat capacity were measured using the laser flash and differential scanning calorimetry methods.

The PbTe and Sn_{0.9}Pb_{0.1}Te materials produced using extrusion and spark plasma sintering prove to be single-phase and have homogeneous compositions. For comparable synthesis methods, the dislocation density in the Sn_{0.9}Pb_{0.1}Te specimens is by an order of magnitude lower than in the PbTe ones.

Study of the mechanical properties of *n* and *p* conductivity type specimens over a wide temperature range from 20 to 500 °C has shown that their deformation is plastic and has no traces of brittle fracture. For these plastic materials, the strength criterion has been accepted to be the arbitrary yield stress corresponding to the stress at a 0.2% deformation. The 20 °C yield stress of PbTe and Sn_{0.9}Pb_{0.1}Te is far higher for the specimens produced by extrusion. For all the test temperatures and synthesis methods the Sn_{0.9}Pb_{0.1}Te specimens have a higher strength than the PbTe ones.

The PbTe and Sn_{0.9}Pb_{0.1}Te specimens produced by extrusion have better thermoelectric properties than the spark plasma sintered ones. The heat conductivity of the PbTe and Sn_{0.9}Pb_{0.1}Te specimens is almost the same regardless of compaction method.

Keywords

thermoelectric materials, lead telluride, tin telluride, dynamic compaction, heat conductivity, thermoelectric efficiency

1. Introduction

The abundance of both manmade and natural exhaust heat sources offers a wide range of opportunities for thermoelectric heat conversion to electric power [1–4]. However, wide application of thermoelectric energy converters is currently limited by the insufficient efficiency of thermoelectric devices. The dependence of thermoelectric device efficiency on material properties is expressed through the dimensionless thermoelectric efficiency

$$ZT = \frac{\alpha^2 \sigma}{\kappa},$$

where T is the working temperature, Z is the thermoelectric efficiency, α is the Seebeck coefficient, σ is the electrical conductivity and κ is the heat conductivity.

Thermoelectric materials exhibit the maximum efficiency value ZT_{\max} in a relatively narrow temperature range, whereas the actual operation temperature range of thermoelectric materials is far wider. Depending on the temperature T_{\max} , the thermoelectric materials are divided into low-, medium- and high-temperature ones [5–7]. The low-temperature thermoelectric materials are those having the maximum thermoelectric efficiency at below 300 °C. The working range of the medium-temperature thermoelectric materials is 300 to 600 °C. The high-temperature thermoelectric materials are used at above 600 °C. No thermoelectric materials can provide sufficiently high ZT in the entire temperature range. Therefore for achieving a wide operation temperature range of high-efficiency thermoelectric generators, their design comprises segmented thermoelectric cells. The cell segments are made from different thermoelectric materials each of which has the highest efficiency in its specific temperature range [8–11]. Thermoelectric energy converters find demand in renewable sources (hybrid photo-thermoelectric solar cells, thermoelectric generators for low-grade heat recovery from geothermal sources, thermoelectric generators driven by temperature difference between water or ice layers at different depths of seas and oceans etc.). However, the most promising application domain of thermoelectric generators is currently the electric power conversion of waste heat from units of cars and other vehicles, as well as electric power plants and industrial installations. The most promising operation temperature range for thermoelectric generators, primarily, those recovering exhaust heat, is 300 to 600 °C [12]. The main thermoelectric material for this range is lead telluride (PbTe) and solid solutions on its basis [16–18].

Thermoelectric materials, especially those used in electric power generators, may undergo mechanical stresses produced at sufficiently large temperature differences between the hot and cold ends of the thermoelectric cell [19]. In that case, a significant additional source of thermal stresses is the difference in the thermal expansion coefficients of materials of directly contacting adjacent segments [20]. It is therefore important to know the

strength parameters of thermoelectric materials having relatively high thermoelectric efficiencies in their respective temperature ranges. There are only a quite limited number of studies dealing with the mechanical properties of medium-temperature thermoelectric materials [21]. The available literary data on the strength of thermoelectric materials mainly refer to low-temperature thermoelectric materials based on bismuth and antimony telluride solid solutions [22, 23].

This work presents dynamic uniaxial compression test data on the temperature dependences of the mechanical properties of PbTe and $\text{Sn}_{0.9}\text{Pb}_{0.1}\text{Te}$ medium-temperature thermoelectric materials having n and p conductivity types, respectively.

2. Experimental

PbTe and $\text{Sn}_{0.9}\text{Pb}_{0.1}\text{Te}$ medium-temperature thermoelectric materials were synthesized by direct smelting of raw components taken in the stoichiometric ratio at 1000 °C for 4 h. The synthesized material was crushed to a powder size of 500±40 μm. The specimens were produced by powder compression using the hot extrusion and spark plasma sintering (SPS) methods. Hot extrusion was carried out under a 100-ton hydraulic press at 400–420 °C, 400–500 MPa and an extrusion coefficient of 9. SPS was conducted at 450 °C, 80 MPa and 5 min exposure at the temperature plateau. The specimens for uniaxial compression tests had dimensions of 5 × 5 × 6 mm³.

The mechanical tests were conducted on an Instron 5982 universal automatic tester controlled by the Bluehill Materials Testing Software. The specimen load measuring error was within 0.4% of current readings. The compression tests were carried out at a constant traverse speed of 0.05 mm/min, the path measuring error being ±0.001 mm. The specimens were heated with a hanging split electric oven, the specimen temperature being measured with a Chromel-Alumel thermocouple.

The phase compositions of the specimens were studied using X-ray diffraction on a Bruker D8 diffractometer in CuK_α radiation. The structural element sizes of the PbTe and $\text{Sn}_{0.9}\text{Pb}_{0.1}\text{Te}$ specimens were studied on cleaves using scanning electron microscopy under a JSM-6480LV microscope. The cleaves were made at room temperature. The secondary electron images were produced at a 30 kV acceleration voltage.

The electrical conductivities and Seebeck coefficients of the specimens were measured simultaneously using the four-probe and differential methods with an Ulvac ZEM-3 instrument. The heat conductivity was calculated using the formula

$$\kappa = D_t C_p d,$$

where D_t is the temperature conductivity, C_p is the specific heat capacity and d is the density. The temperature conductivity and the specific heat capacity were measured

using laser flash and differential scanning calorimetry methods on LFA 457 (Netzsch) and DSC-404C (Netzsch) plants, respectively. The density of the specimens was measured using Archimedes' method.

3. Results and discussion

According to X-ray diffraction data, the PbTe polycrystalline specimens produced by SPS and extrusion were single-phase. The diffraction maximum intensities suggest that the test specimens had no preferential grain orientations (Fig. 1). The coherent region sizes (CRS) and microdeformations were assessed from diffraction peak broadening. Regardless of production method, diffraction peak broadening for the PbTe specimens was only caused by microdeformations originating from randomly distributed dislocations. The CRS were greater than 200 nm and did not contribute to diffraction peak broadening. The dislocation density in the PbTe specimens produced by SPS was $4 \cdot 10^5 \text{ cm}^{-2}$. The dislocation density in the PbTe specimens produced by extrusion was $2 \cdot 10^7 \text{ cm}^{-2}$.

The *p* conductivity type materials produced by SPS and extrusion also were single-phase and had no texture. The diffraction patterns of the *p* conductivity type specimens contained only peaks of the $\text{Sn}_{1-x}\text{Pb}_x\text{Te}$ solid solution. Solid solution stratification or component segregation were not observed in the compacted specimens. The composition of the $\text{Sn}_{1-x}\text{Pb}_x\text{Te}$ solid solution as determined from lattice parameters was stoichiometric, i.e., $\text{Sn}_{0.9}\text{Pb}_{0.1}\text{Te}$. The solid solution composition was homogeneous. The dislocation densities assessed from dislocation peak broadening were $5 \cdot 10^4$ and $3 \cdot 10^6 \text{ cm}^{-2}$ for the SPS and extrusion $\text{Sn}_{0.9}\text{Pb}_{0.1}\text{Te}$ specimens, respectively.

Thus the initial polycrystalline sintered and hot extruded PbTe and $\text{Sn}_{0.9}\text{Pb}_{0.1}\text{Te}$ specimens were single-phase and had no preferential grain orientations. The dislocation density in the extruded specimens was higher than in the SPS specimens. Comparison between the structures

of the PbTe and $\text{Sn}_{0.9}\text{Pb}_{0.1}\text{Te}$ specimens produced using the same method showed that the dislocation density in the $\text{Sn}_{0.9}\text{Pb}_{0.1}\text{Te}$ specimens is by an order of magnitude lower than in the PbTe specimens.

The less defective structure of the $\text{Sn}_{0.9}\text{Pb}_{0.1}\text{Te}$ specimens as compared with PbTe for the comparable synthesis method can originate from the fact that the homologous temperature at which the specimens were compacted is higher for the SnTe solid solution ($T/T_{\text{melt}} = 0.67$) than for PbTe ($T/T_{\text{melt}} = 0.60$). Therefore the diffusion mobility in $\text{Sn}_{0.9}\text{Pb}_{0.1}\text{Te}$ is higher than in PbTe and hence the defects will be annealed faster and the crystalline structure will be more perfect in the $\text{Sn}_{0.9}\text{Pb}_{0.1}\text{Te}$ specimens than in the PbTe ones regardless of production method.

Figure 2 shows cleavage surface images for the SPS and extruded PbTe and $\text{Sn}_{0.9}\text{Pb}_{0.1}\text{Te}$ specimens. There was no significant difference between the cleavage surface patterns of the specimens produced using different methods. The cleavage textures of the PbTe and $\text{Sn}_{0.9}\text{Pb}_{0.1}\text{Te}$ specimens reflect the grain structure of the materials because secondary electron imaging occurs by electron reflection from different crystal surfaces having different grain cleavage surface orientations. The cleavage surface images of the PbTe and $\text{Sn}_{0.9}\text{Pb}_{0.1}\text{Te}$ specimens clearly show grain facets. The grain shapes are close to isotropic. The images show individual pores located in grain bulk and at grain boundaries. The pore sizes are $\sim 200\text{--}400 \text{ nm}$ for the PbTe and $\text{Sn}_{0.9}\text{Pb}_{0.1}\text{Te}$ specimens produced using different methods, but the extruded PbTe and $\text{Sn}_{0.9}\text{Pb}_{0.1}\text{Te}$ specimens contain more pores than the SPS specimens. Grain sizes as assessed from scanning electron microscopy images for the extruded and SPS PbTe specimens are $\sim 20 \text{ nm}$ and 25 nm , respectively. The grains in the $\text{Sn}_{0.9}\text{Pb}_{0.1}\text{Te}$ specimens are larger than in PbTe produced using the same method. The average pore size in the extruded $\text{Sn}_{0.9}\text{Pb}_{0.1}\text{Te}$ specimen was $\sim 35 \text{ nm}$ and that in the SPS specimen, $\sim 40 \text{ nm}$.

Figure 3 shows the deformation curves of the extruded and SPS PbTe specimens. The curves suggest that at 20

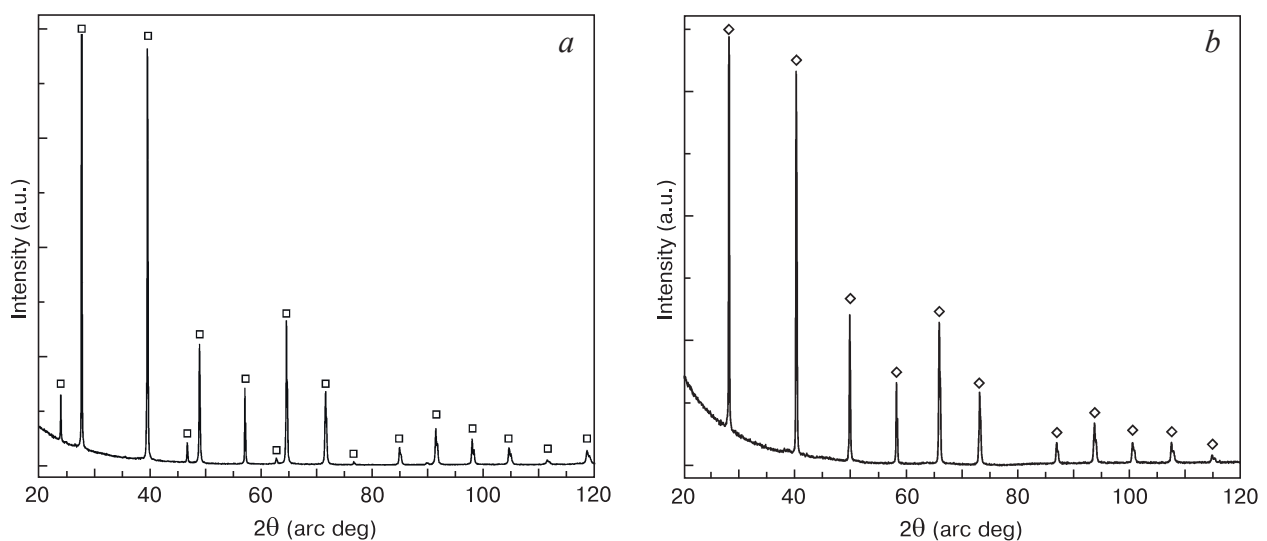


Figure 1. Diffraction patterns of (a) PbTe and (b) $\text{Sn}_{1-x}\text{Pb}_x\text{Te}$ specimens produced using SPS

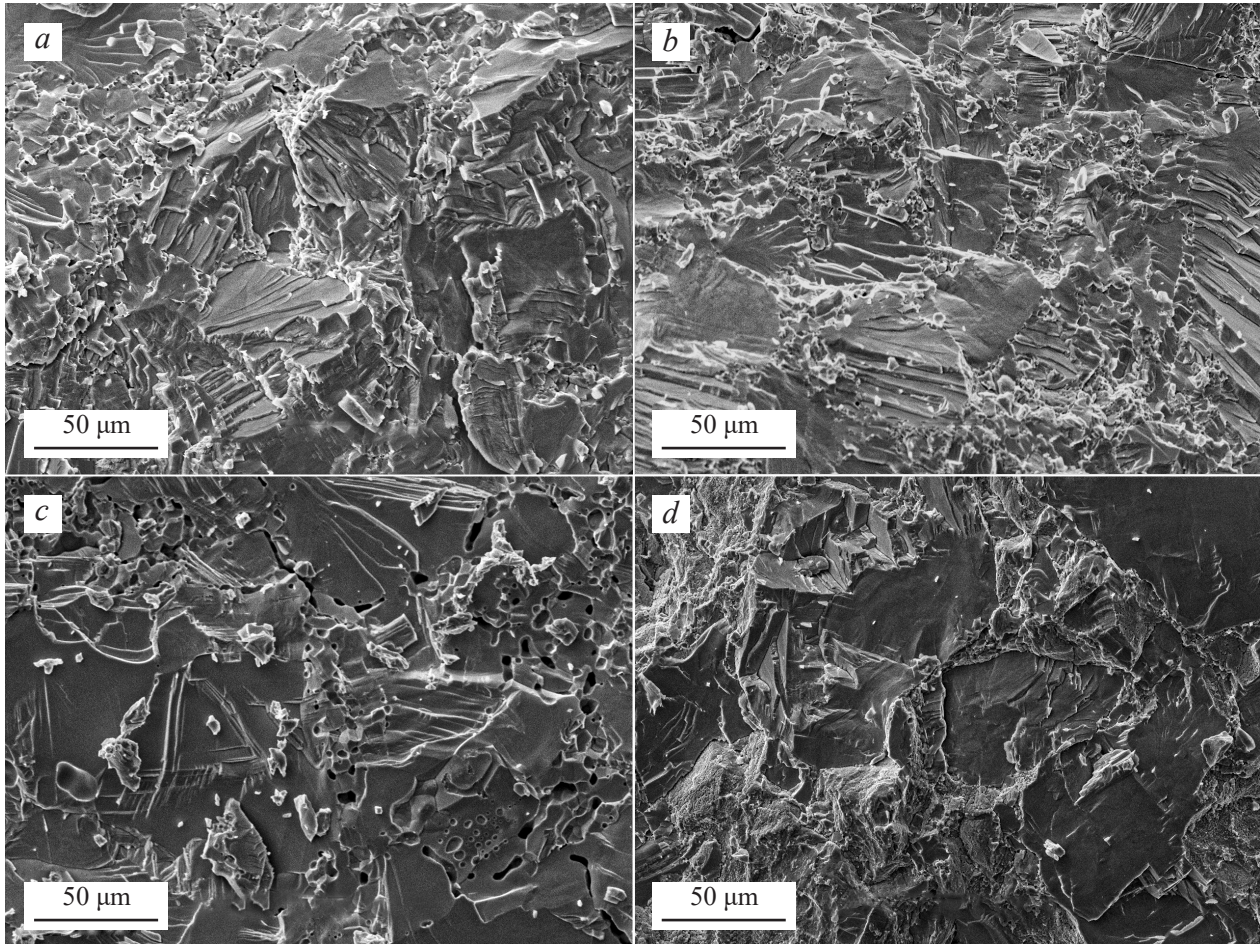


Figure 2. Cleavage surface images of (a and b) PbTe and (c and d) Sn_{0.9}Pb_{0.1}Te specimens produced by (a and c) extrusion and (b and d) SPS

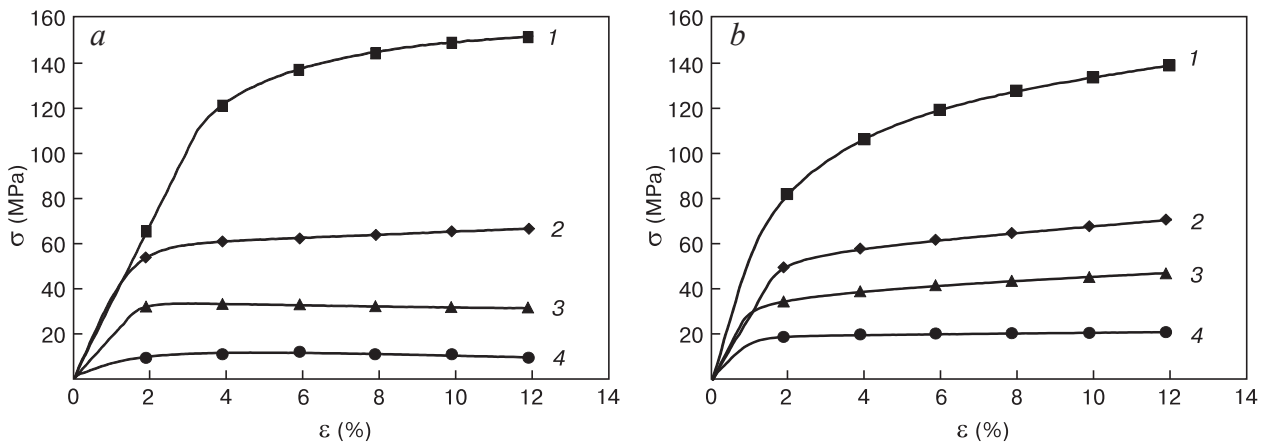


Figure 3. Diffraction patterns of (a) extruded and (b) SPS PbTe specimens at temperatures: (1) 20 °C; (2) 200 °C; (3) 300 °C; (4) 500 °C

to 500 °C the deformation to as high as $\epsilon = 12\%$ remains plastic: the linear stress vs deformation curve in the elastic region changes to plastic flow at greater deformations. This is the fundamental difference between these specimens and the low-temperature Bi₂Te₃ based solid solutions in which a brittle-ductile transition occurs at below 200 °C. Deformation of the extruded and SPS PbTe specimens at below 300 °C has a deformation hardening region

without fracture, this region being more expressed for the SPS specimens. In this case, estimation of the materials' yield stress would be incorrect. However, assessing the strength of the specimens from their maximum stress during deformation, one can conclude that it is almost insensitive to material production method. Mechanical stresses in the PbTe specimens reach their maximum values of ~149 MPa at room temperature. With an increase in the

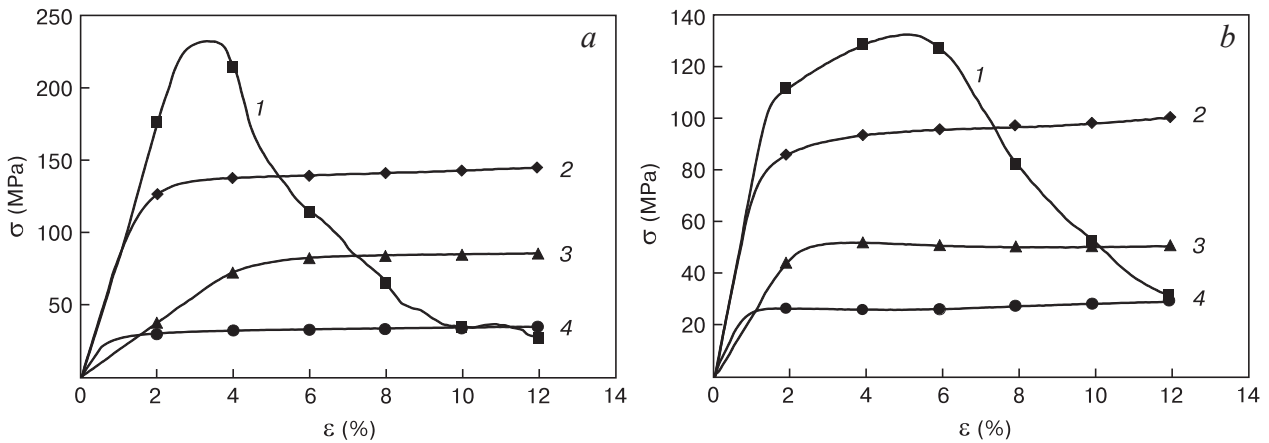


Figure 4. Diffraction patterns of (a) extruded and (b) SPS $\text{Sn}_{0.9}\text{Pb}_{0.1}\text{Te}$ specimens at temperatures: (1) 20 °C; (2) 200 °C; (3) 300 °C; (4) 500 °C

test temperature to 200 °C, σ_{max} decreases by two times to 70 MPa. With a further increase in temperature the evolution pattern of σ_{max} remains the same.

Figure 4 shows the deformation curves of the extruded and SPS $\text{Sn}_{0.9}\text{Pb}_{0.1}\text{Te}$ specimens. It can be seen from Fig. 4 that deformation of $\text{Sn}_{0.9}\text{Pb}_{0.1}\text{Te}$ is also plastic over a wide temperature range. The only exclusion is room temperature at which the deformation curve has an elastic/plastic pattern: the stress is the highest in a region of relatively low deformations which is at 2–4% for the extruded

specimens and 4–6% for the SPS ones, following which the specimens undergo softening which however does not cause complete fracture. This is most probably because microstacks or twins form during 20 °C deformation. The highest mechanical stresses in the $\text{Sn}_{0.9}\text{Pb}_{0.1}\text{Te}$ specimens are achieved, by analogy with PbTe, at room temperature. However, unlike the PnTe specimens for which the production method had no significant effect on σ_{max} , the hot extruded $\text{Sn}_{0.9}\text{Pb}_{0.1}\text{Te}$ specimens have almost twice as high room temperature maximum mechanical

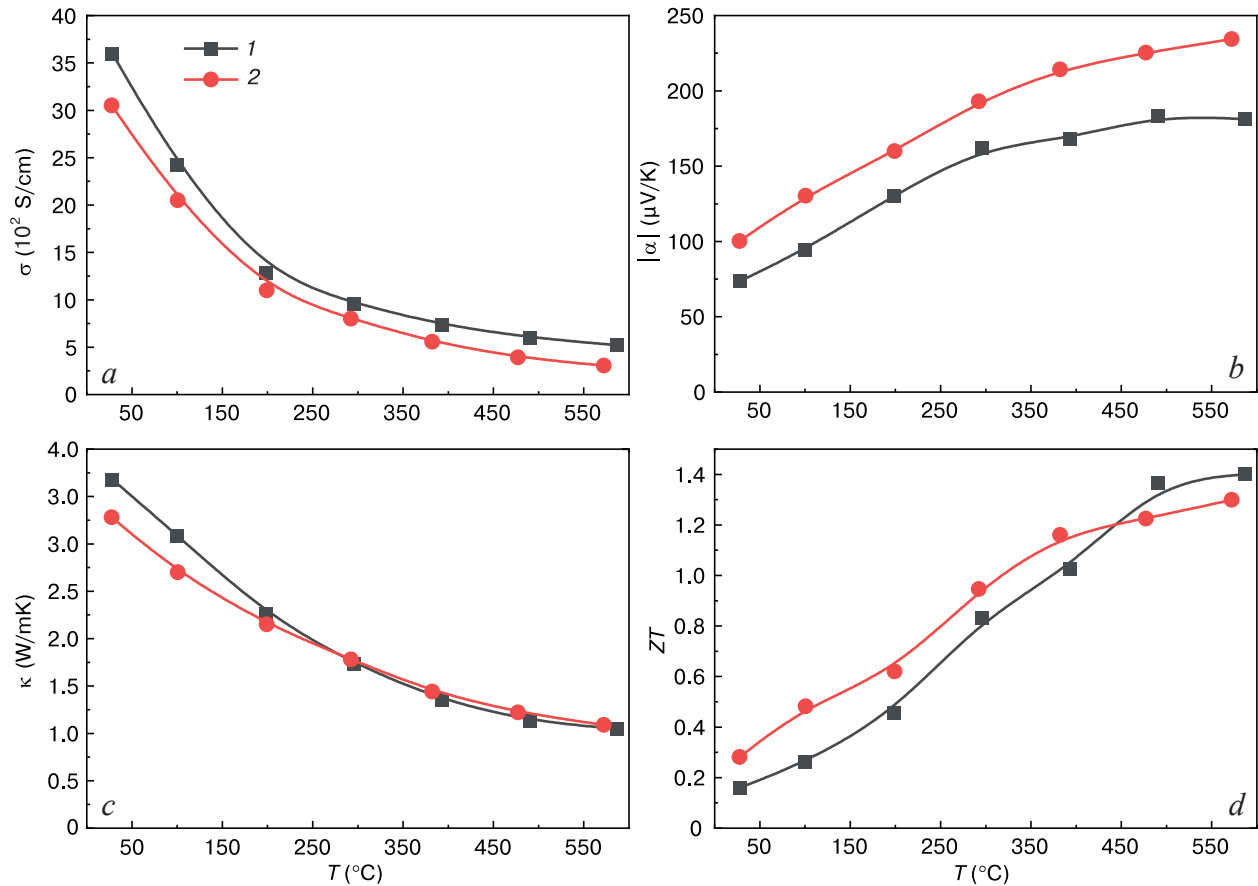


Figure 5. Temperature dependences of (a) electrical conductivity, (b) Seebeck coefficient, (c) heat conductivity and (d) thermoelectric efficiency for (1) extruded and (2) SPS PbTe specimens

stresses as those of the SPS $\text{Sn}_{0.9}\text{Pb}_{0.1}\text{Te}$ specimens. The room temperature σ_{\max} values for the extruded and SPS $\text{Sn}_{0.9}\text{Pb}_{0.1}\text{Te}$ specimens are 240 and 135 MPa, respectively.

Thus, the extruded specimens have the highest room temperature σ_{\max} for both the PbTe and $\text{Sn}_{0.9}\text{Pb}_{0.1}\text{Te}$ materials. This difference decreases with an increase in temperature and then becomes almost zero (at 200 °C for PbTe and at 400 °C for $\text{Sn}_{0.9}\text{Pb}_{0.1}\text{Te}$). This is because an increase in temperature leads to recrystallization making the structure of extruded materials more similar to the structure of SPS materials. σ_{\max} decreases with an increase in temperature more intensely for the extruded specimens. The σ_{\max} vs T curves for PbTe intersect and at above 200 °C the sintered material has but slightly higher strength than the extruded one.

It should be noted that the $\text{Sn}_{0.9}\text{Pb}_{0.1}\text{Te}$ solid solution specimens have a higher strength than the PbTe specimens at any temperature and for all production methods.

Figures 5 and 6 illustrate the thermoelectric properties of the extruded and SPS PbTe and $\text{Sn}_{0.9}\text{Pb}_{0.1}\text{Te}$ specimens.

It can be seen from the data shown in Fig. 5 that the electrical conductivity of the n conductivity type PbTe specimens decreases with an increase in temperature, the electrical conductivity of the extruded material being higher in the entire temperature range than that of the SPS

specimens. The Seebeck coefficients of all the specimens increase with temperature, the SPS PbTe specimens having higher Seebeck coefficients. The heat conductivities of the PbTe specimens decrease with an increase in temperature and are close for the extruded and SPS specimens in the entire temperature range. The thermoelectric efficiency of SPS PbTe is higher than that of the extruded specimens in the 25 to 200 °C range. However, at 400–600 °C range which is the working one for medium-temperature thermoelectric materials the hot extruded PbTe specimens have higher thermoelectric efficiencies. At 600 °C the thermoelectric efficiencies of the extruded and SPS specimens are ~ 1.4 and ~ 1.3 , respectively. Thus the electrical conductivity of the PbTe specimens is almost insensitive to compaction method. The electrical conductivity of the extruded specimens is higher, possibly due to the formation of point defects during extrusion which increase the concentration of majority carriers.

The temperature dependences of the electrical conductivity and the Seebeck coefficient of the p conductivity type $\text{Sn}_{0.9}\text{Pb}_{0.1}\text{Te}$ specimens have a similar pattern to those of PbTe (Fig. 6). However, in contrast to the n conductivity type, the electrical conductivity of the SPS $\text{Sn}_{0.9}\text{Pb}_{0.1}\text{Te}$ specimens is higher than that of the extruded specimens in almost the whole temperature range. Accordingly, the Seebeck coefficients of the SPS $\text{Sn}_{0.9}\text{Pb}_{0.1}\text{Te}$ specimens are lower than those of the hot extruded $\text{Sn}_{0.9}\text{Pb}_{0.1}\text{Te}$

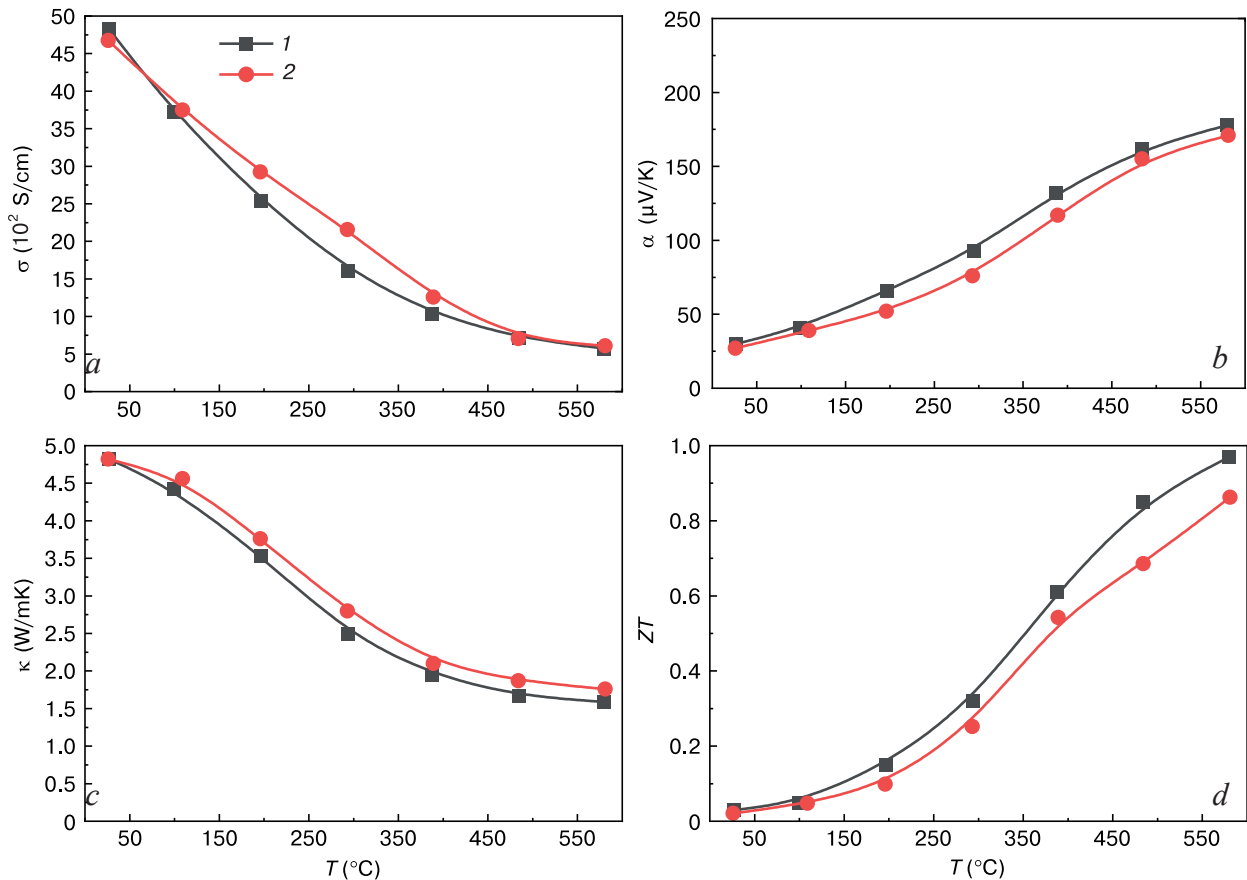


Figure 6. Temperature dependences of (a) electrical conductivity, (b) Seebeck coefficient, (c) heat conductivity and (d) thermoelectric efficiency for (1) extruded and (2) SPS $\text{Sn}_{0.9}\text{Pb}_{0.1}\text{Te}$ specimens

specimens. This difference in the behavior of the electro-physical properties between the specimens produced by extrusion and SPS is caused by the formation of point defects during extrusion which have different effects on the concentration of majority carriers in n and p conductivity type thermoelectric materials. The heat conductivities of all the $\text{Sn}_{0.9}\text{Pb}_{0.1}\text{Te}$ specimens are close and, same as for the PbTe specimens, are insensitive to the compaction method used. The thermoelectric efficiencies of the extruded $\text{Sn}_{0.9}\text{Pb}_{0.1}\text{Te}$ specimens are higher than those of the SPS specimens in the entire temperature range. The 600 °C thermoelectric efficiencies of the extruded and SPS specimens are 1.0 and 0.9, respectively.

4. Conclusion

The mechanical properties of medium-temperature PbTe and $\text{Sn}_{0.9}\text{Pb}_{0.1}\text{Te}$ thermoelectric materials produced by extrusion and spark plasma sintering were studied. Regardless of production method, the PbTe and $\text{Sn}_{0.9}\text{Pb}_{0.1}\text{Te}$ specimens are single-phase and have no preferential grain orientations. The dislocation density in the extruded specimens is noticeably higher than in the spark plasma sintered specimens. Comparison of the structural parameters between the n and p conductivity type specimens showed that the structure of the $\text{Sn}_{0.9}\text{Pb}_{0.1}\text{Te}$ specimens is less defective than that of PbTe .

Study of the strength parameters of the specimens as a function of dynamic uniaxial compression temperature showed that deformation in a wide temperature range from 20 to 500 °C is plastic and has no traces of brittle fracture. We showed that the room temperature yield stresses are higher for the extruded specimens and that a decrease in the maximum stress with an increase in temperature is more intense in the extruded specimens; as a result, at above 200 °C the spark plasma sintered material acquires a higher strength than the extruded one.

Regardless of production method the strength parameters of the n conductivity type specimens are higher than those of the p conductivity type PbTe specimens in the entire temperature range.

The extruded PbTe and $\text{Sn}_{0.9}\text{Pb}_{0.1}\text{Te}$ specimens have better thermoelectric properties than the spark plasma sintered specimens. The heat conductivities of the PbTe and $\text{Sn}_{0.9}\text{Pb}_{0.1}\text{Te}$ specimens are almost insensitive to compaction method. The 600 °C thermoelectric efficiencies ZT of PbTe and $\text{Sn}_{0.9}\text{Pb}_{0.1}\text{Te}$ were ~ 1.4 and 1.0, respectively.

Acknowledgements

The work was conducted within State Assignment of the Kurchatov Institute Research Center.

References

1. Hooshmand Zaferani S., Jafarian M., Vashae D., Ghomashchi R. Thermal management systems and waste heat recycling by thermoelectric generators – an overview. *Energies*. 2021; 14(18): 5646. <https://doi.org/10.3390/en14185646>
2. Luo D., Sun Z., Wang R. Performance investigation of a thermoelectric generator system applied in automobile exhaust waste heat recovery. *Energy*. 2022; 238: 121816. <https://doi.org/10.1016/j.energy.2021.121816>
3. Burnete N.V., Mariasiu F., Depeik C., Barabas I., Moldovanu D. Review of thermoelectric generation for internal combustion engine waste heat recovery. *Progress in Energy and Combustion Science*. 2022; 91(01): 101009. <https://doi.org/10.1016/j.pecs.2022.101009>
4. Champier D. Thermoelectric generators: a review of applications. *Energy Conversion and Management*. 2017; 140: 167–181. <https://doi.org/10.1016/j.enconman.2017.02.070>
5. Zhang X., Zhao L.-D. Thermoelectric materials: Energy conversion between heat and electricity. *Journal of Materiomics*. 2015; 1(2): 92–105. <https://doi.org/10.1016/j.jmat.2015.01.001>
6. Wei J., Yang L., Ma Z., Song P., Zhang M., Ma J., Yang F., Wang X. Review of current high-ZT thermoelectric materials. *Journal of Materials Science*. 2020; 55: 12642–12704. <https://doi.org/10.1007/s10853-020-04949-0>
7. Shtern M., Rogachev M., Shtern Yu., Sherchenkov A., Babich A., Korchagin E., Nikulin D. Thermoelectric properties of efficient thermoelectric materials on the basis of bismuth and antimony chalcogenides for multisection thermoelements. *Journal of Alloys and Compounds*. 2021; 877: 160328. <https://doi.org/10.1016/j.jallcom.2021.160328>
8. Ngan P.H., Christensen D.V., Snyder G.J., Hung L.T., Linderoth S., Nong N.V., Pryds N. Towards high efficiency segmented thermoelectric unicouples. *Advanced Materials Physics*. 2014; 211(1): 9–17. <https://doi.org/10.1002/pssa.201330155>
9. Shtern M.Yu., Rogachev M.S., Sherchenkov A.A., Shtern Yu.I. Development and investigation of the effective thermoelectric materials for the multisectional generator thermoelements. *Materialstoday: Proceedings*. 2020; 20(Pt 3): 295–304. <https://doi.org/10.1016/j.matpr.2019.10.066>
10. Li W., Poudel B., Nozariasbarmar A., Sriramdas R., Zhu H., Kang H.B., Priya S. Bismuth telluride/half-heusler segmented thermoelectric uncouple modules provide 12% conversion efficiency. *Advanced Energy Materials*. 2020; 10(38): 2001924. <https://doi.org/10.1002/aenm.202001924>
11. Zhao J., Xu W., Kuang Z., Long R., Liu Z., Liu W. Segmental material design in thermoelectric devices to boost heat-to-electricity per-

- fomance. *Energy Conversion and Management*. 2021; 247: 114754. <https://doi.org/10.1016/j.enconman.2021.114754>
12. Das Raghu. Thermoelectric Energy Harvesting 2014-2024: Devices, Applications, Opportunities. *IDTechEx*. 2014; 96.
 13. Goldsmid H.J. Bismuth telluride and its alloys materials for thermoelectric generation. *Materials*. 2014; 7(4): 2577–2592. <https://doi.org/10.3390/ma7042577>
 14. Maksymuk M., Parashchuk T., Dzundza B., Nykyriy L., Chernyak L., Dashevsky Z. Highly efficient bismuth telluride-based thermoelectric microconverters. *Materials Today Energy*. 2021; 21: 100753. <https://doi.org/10.1016/j.mtener.2021.100753>
 15. Zulkepli N., Yunas J., Mohamed M.A., Hamzah A.A. Review of thermoelectric generators at low operating temperatures: working principles and materials. *Micromachines*. 2021; 12(7): 734. <https://doi.org/10.3390/mi12070734>
 16. Su Ch.-H. Design, growth and characterization of PbTe-based thermoelectric materials. *Progress in Crystal Growth and Characterization of Materials*. 2019; 65(2): 47–94. <https://doi.org/10.1016/j.pcrysgrow.2019.04.001>
 17. Shtern Yu., Sherchenkov A., Shtern M., Rogachev M., Pepelyaev D. Challenges and perspective recent trends of enhancing the efficiency of thermoelectric materials on the basis of PbTe. *Materialstoday: Communications*. 2023; 37: 107083. <https://doi.org/10.1016/j.mtcomm.2023.107083>
 18. Knura R., Parashchuk T., Yoshiasa A., Wojciechowski K.T. Origins of low lattice thermal conductivity of $Pb_{1-x}Sn_xTe$ alloys for thermoelectric applications. *Dalton Transactions*. 2021; 50: 4323. <https://doi.org/10.1039/D0DT04206D>
 19. Maduabuchi C. Thermo-mechanical optimization of thermoelectric generators using deep learning artificial intelligence algorithms fed with verified finite element simulation data. *Applied Energy*. 2022; 315(1): 118943. <https://doi.org/10.1016/j.apenergy.2022.118943>
 20. Lee M.-Y., Seo J.-H., Lee H.-S., Garud K.S. Power generation, efficiency and thermal stress of thermoelectric module with leg geometry, material, segmentation and two-stage arrangement. *Symmetry*. 2020; 12(5): 786. <https://doi.org/10.3390/sym12050786>
 21. Shtern M., Sherchenkov A., Shtern Yu., Borgardt N., Rogachev M., Yakubov A., Babich A., Pepelyaev D., Voloshchuk I., Zaytseva Yu., Pereverzeva S., Gerasimenko A., Potapov D., Murashko D. Mechanical properties and thermal stability of nanostructured thermoelectric materials on the basis of PbTe and GeTe. *Journal of Alloys and Compounds*. 2023; 946: 169364. <https://doi.org/10.1016/j.jallcom.2023.169364>
 22. Lavrentev M.G., Osvenskii V.B., Parkhomenko Y.N., Pivovarov G.I., Sorokin A.I., Bulat L.P., Kim H.-S., Witting I.T., Snyder G.J., Bublik V.T., Tabachkova N.Y. Improved mechanical properties of thermoelectric $(Bi_{0.2}Sb_{0.8})_2Te_3$ by nanostructuring. *APL Letters*. 2016; 4(10): 104807. <https://doi.org/10.1063/1.4953173>
 23. Zhu Yu., Wu P., Guo J., Zhou Y., Chong X., Ge Z., Feng J. Achieving a fine balance in mechanical properties and thermoelectric performance in commercial Bi_2Te_3 materials. *Ceramics International*. 2020; 46(10 (Pt A)): 14994–15002. <https://doi.org/10.1016/j.ceramint.2020.03.029>